Synaptic transmission onto hippocampal glial cells with hGFAP promoter activity

Ronald Jabs[1,*], Tatjana Pivneva[2], Kerstin Hüttmann[1], Alexandra Wyczynski[1], Christiane Nolte[3], Helmut Kettenmann[3] and Christian Steinhäuser[1]

[1]Experimental Neurobiology, Department of Neurosurgery, University of Bonn, Sigmund-Freud-Str. 25, 53105 Bonn, Germany
[2]Bogomoletz Institute of Physiology, Bogomoletz St. 4, 01024 Kiev, Ukraine
[3]Cellular Neurosciences, Max Delbrück Center for Molecular Medicine, Berlin, Robert Rössle Str., Germany
*Author for correspondence (e-mail: ronald.jabs@ukb.uni-bonn.de)

Accepted 26 May 2005
Journal of Cell Science 118, 3791-3803 Published by The Company of Biologists 2005
doi:10.1242/jcs.02515

Summary

Glial cells increasingly gain importance as part of the brain's communication network. Using transgenic mice expressing green fluorescent protein (EGFP) under the control of the human GFAP promoter, we tested for synaptic input to identified glial cells in the hippocampus. Electron microscopic inspection identified synapse-like structures with EGFP-positive postsynaptic compartments. Sub-threshold stimulation to Schaffer collaterals resulted in stimulus-correlated, postsynaptic responses in a subpopulation of EGFP-positive cells studied with the patch-clamp technique in acute slices. This cell population can be recognized by its distinct morphology and has been termed GluR cells in a preceding study. These cells are distinct from the classical astrocytes due to their antigen profile and functional properties, but also lack characteristic features of oligodendrocytes or neurons. GluR cells also received spontaneous synaptic input. Stimulus-correlated and spontaneous responses were quantitatively analysed by ascertaining amplitude distributions, failure rates, kinetics as well as pharmacological properties. The data demonstrate that GABAergic and glutamatergic neurons directly synapse onto GluR cells and suggest a low number of neuronal release sites. These data demonstrate that a distinct type of glial cells is integrated into the synaptic circuit of the hippocampus, extending the finding that synapse-based brain information processing is not a property exclusive to neurons.

Supplementary material available online at
http://jcs.biologists.org/cgi/content/full/118/16/3791/DC1

Key words: $GABA_A$ receptor, GFAP, Glia, Glutamate, Hippocampus, Neuron-glia interaction.

Introduction

Recent work on glial cell physiology has disclosed that these cells are much more actively involved in brain information processing than hitherto thought. This new insight stimulates a new view according to which the active brain has to be regarded as an integrated circuit of interactive neurons and glial cells. Astrocytes in particular are now regarded as direct communication partners of neurons, by dynamically interacting with synapses through the uptake and release of neurotransmitters and receptor-mediated intracellular Ca^{2+} signalling (for reviews, see Haydon, 2001; Newman, 2003; Fellin and Carmignoto, 2004; Volterra and Steinhäuser, 2004; Schipke and Kettenmann, 2004). Intriguingly, a distinct subset of glial cells in the hippocampus was reported to receive direct synaptic input from glutamatergic and GABAergic neurons. These glial cells expressed the proteoglycan, NG2, and on this basis were regarded as oligodendrocyte precursor cells (OPCs) (Bergles et al., 2000; Lin and Bergles, 2003). However, the identity of these cells needs further consideration because the specificity of NG2 as an OPC marker becomes increasingly questionable. Current work suggests that NG2 cells comprise a distinct, heterogeneous type of neuroglial cells (Nishiyama et al., 2002; Stallcup, 2002; Greenwood and Butt, 2003; Aguirre et al., 2004; Peters, 2004).

Using transgenic mice expressing green fluorescent protein under control of the human GFAP promoter (hGFAP/EGFP mice), we have recently reported a co-existence of two types of glial cells in the hippocampus, distinguishable from each other by mutually exclusive expression of glutamate transporters (GluT type) and ionotropic glutamate receptors (GluR cells). GluT type cells were extensively coupled via gap junctions and contacted blood vessels, thus matching properties of classical astrocytes. By contrast, GluR cells lacked junctional coupling and did not enwrap capillaries (Matthias et al., 2003; Wallraff et al., 2004). Moreover, GluR cells co-expressed S100β, a common astrocyte marker, NG2, as well as neuronal genes, and hence escaped classification into neurons, astrocytes, or oligodendrocytes.

Here we used the hGFAP/EGFP transgenic animal to identify distinct types of glial cells in live slices. We combined ultrastructural analysis and post-recording immunocytochemistry to test whether the two populations of hGFAP/EGFP-positive glial cells in the hippocampus receive synaptic input. Electron microscopic inspection identified synapse-like structures with EGFP-positive postsynaptic compartments. Patch clamp recordings revealed stimulus-

correlated as well as spontaneous postsynaptic events in GluR cells, but not in GluT cells.

Materials and Methods

Immuno-electron microscopy

Preparing tissue for pre-embedding techniques

hGFAP/EGFP transgenic mice (Nolte et al., 2001) (6-12 weeks old; *n*=8 for HRP reaction, *n*=6 for silver-enhancement technique) were anesthetized deeply by pentobarbital and perfused intra-cardially with 4% paraformaldehyde, 0.25% glutaraldehyde in 0.1 M phosphate buffer (PB; pH 7.4). Brains were removed, post-fixed overnight at 4°C and subsequently rinsed in cold PB.

Vibratome sections (30-40 μm thickness) were cut perpendicularly to the longitudinal axis of the hippocampus on a Vibracut (FTB Feinwerktechnik, Bensheim, Germany). After permeabilization with 0.1% Triton X-100 and inactivation of endogenous peroxidase (latter step only for slices to be processed with HRP-coupled secondary antibodies), vibratome sections were incubated for 48 hours at 4°C with anti-GFP antibodies (rabbit IgG fraction, Molecular Probes, MoBitec, Göttingen, Germany) diluted 1:500 in blocking solution [5% BSA, 5% normal goat serum (NGS) in 0.1 M PB]. As controls, primary antibodies were omitted and slices were incubated in blocking solution. After extensive rinsing in PB, slices were incubated either with peroxidase-conjugated goat anti-rabbit IgG (1:200) (Dianova, Hamburg, Germany) or with goat anti-rabbit IgG conjugated to 1.4 nm gold (Nanogold; Nanoprobes, Yaphank, NY, USA) (1:40) for overnight at room temperature. After rinsing, slices incubated with HRP-conjugated secondary antibodies were developed using the standard diaminobenzidine (DAB) reaction. Slices probed with nanogold-coupled secondary antibodies underwent silver-intensified pre-embedding immunogold reaction as described (Baude et al., 1993). Subsequently, slices were post-fixed in osmium tetroxide, dehydrated in increasing series of ethanol, pre-embedded with propylene oxide and flat embedded in epoxy resin (agar 100 resin, araldite CY 212, DDSA, DMP-30; Plano, Wetzlar, Germany). Ultrathin sections were stained with uranyl acetate and lead citrate and examined with a Philips 400 electron microscope at 80 kV or a JEOL 100CX electron microscope at 60 kV.

Post-embedding immunocytochemistry

hGFAP/EGFP transgenic mice (*n*=6) were perfused intra-cardially as described above with the following fixative: 4% paraformaldehyde, 0.05% glutaraldehyde and 0.2% of picric acid in 0.1 M PB (pH 7.4). After 15 minutes perfusion, the brains were removed, 500 μm thick vibratome sections were cut and sections were washed several times in PB. Freeze substitution and low temperature embedding in acrylic resins were carried out as described earlier (Baude et al., 1995; Nusser et al., 1997). For cryoprotection, slices were placed into sucrose solutions (concentration 0.5-2.0 M) in 0.05 M Tris-maleat buffer. They were then slammed onto copper blocks cooled in liquid N_2, followed by freeze-substitution with methanol and embedding in Lowicryl HM 20 (Chemische Werke Lowi GMBH, Germany) resins.

Lowicryl resin-embedded ultrathin sections (75-90 nm thickness) were picked up on formvar-coated copper grids and were incubated on drops of blocking solution consisting of TBS (50 mM Tris-HCl, pH 7.4, 0.3% NaCl) and 10% of NGS. Primary, anti-GFP antibodies (rabbit IgG, MoBiTec) were diluted 1:50 in TBS containing 2% NGS and sections were incubated on drops of antibody solution overnight at 4°C. Subsequently, sections were washed and incubated for 40 minutes with secondary antibodies (goat anti-rabbit IgG coupled to 12 nm colloidal gold; 1:100; Immunotech, Dianova). After several washing steps in PB and in ultra-pure water, the sections were contrasted with saturated aqueous uranyl acetate followed by staining with lead citrate. As a control, primary antibodies were either omitted and slices were incubated in blocking solution or replaced by 5% normal rabbit serum.

Slice preparation for electrophysiology and immunohistochemistry

Transgenic hGFAP/EGFP mice aged p9-p12 were anaesthetized, decapitated, the brains were removed. Hippocampal slices (300 μm) were cut perpendicularly to the main hippocampal axis using ice-cold oxygenated solution consisting of (in mM): 87 NaCl, 2.5 KCl, 1.25 NaH_2PO_4, 7 $MgCl_2$, 0.5 $CaCl_2$, 25 $NaHCO_3$, 25 glucose, 75 sucrose (347 mOsmol). The slices were stored for 30 minutes in the same solution at 35°C and then transferred into artificial cerebrospinal fluid (aCSF) containing (in mM): 126 NaCl, 3 KCl, 2 $MgSO_4$, 2 $CaCl_2$, 10 glucose 1.25 NaH_2PO_4, 26 $NaHCO_3$, equilibrated with 95% O_2 and 5% CO_2 to a pH of 7.4 at room temperature.

Patch-clamp recordings

Slices were transferred to a recording chamber, and were constantly perfused with aCSF at room temperature. Whole-cell recordings were obtained using an EPC8 amplifier (HEKA Elektronik, Lambrecht, Germany). The holding potential in the voltage clamp mode was –80 mV, if not stated otherwise. In the current clamp mode, voltage signals were additionally amplified with a DPA 2F amplifier (NPI electronic GmbH, Tamm, Germany). Signals were digitized with an ITC 16 (NPI electronic). Patch pipettes, fabricated from borosilicate capillaries (Hilgenberg, Malsfeld, Germany), had resistances of 3-6 MΩ when filled with a solution consisting of (in mM): 130 KCl, 2 $MgCl_2$, 0.5 $CaCl_2$, 3 Na_2-ATP, 5 BAPTA, 10 HEPES. Experiments displayed in Figs 6-8 were performed with 125 K-gluconate, 20 KCl, 3 NaCl, 2 Na_2-ATP, 2 $MgCl_2$, 0.5 EGTA, 10 HEPES. The pH was adjusted to 7.25 for both internal solutions. Voltages were corrected for liquid junction potential (6 mV for the K-gluconate solution). Recordings were monitored with TIDA software (HEKA). Series and membrane resistance were checked in constant intervals with self-customized macros using Igor Pro 5.03 software (WaveMetrix Inc., Lake Oswedo, USA). Visual control was achieved with a microscope equipped with an infrared DIC system (Axioskop FS2, Zeiss, Oberkochen, Germany) and a 60× LUMPlan FI/IR objective (Olympus Optical Co., Hamburg, Germany). The infrared image was captured with an analogue tube camera and contrast enhanced with a controller (C2400-07, Hamamatsu Photonics, Herrsching am Ammersee, Germany).

Stimulation of neuronal fibers and field potential recordings

Schaffer collaterals were stimulated with bipolar electrodes (TST33C0, WPI Inc., Sarasota, USA). Pulse sequences were generated with a Master 8 device (A.M.P.I., Jerusalem, Israel) and applied with a constant current stimulus isolator (A360, WPI). Experiments depicted in Fig. 8 were performed with an AM-Systems isolation pulse stimulator (model 2100, Jerusalem, Israel) in the constant voltage mode. In parallel to whole-cell patch clamp measurements, extracellular field potentials were recorded with a SEC-05 LX amplifier (NPI electronic) in the bridge mode (aCSF-filled glass pipette). Stimulation pulse duration and intensity, ranging between 50-200 μs and 50-200 μA, was adjusted to obtain only sub-threshold field potentials. Field potentials were additionally amplified with a DPA 2F amplifier (NPI electronic). The postsynaptic currents (PSCs) shown in Figs 6-8 were evoked by near field stimulation. A low resistance (<1 MΩ), aCSF filled glass capillary was used as a monopolar stimulation electrode. It was positioned close to the patch electrode and moved under optical control to optimise PSC recordings. The GluR cells tested in this study displayed an input resistance of R_i=232±253 MΩ, a membrane capacitance of C_m= 29±14 pF, and a resting potential of V_{rest}=–82±6 mV (*n*=57). The

corresponding data for GluT cells were R_i=8.1±6.5 MΩ, C_m=76±43 pF, and V_{rest}=–82±4 mV (*n*=38).

Offline compensation of capacitative artefact

Membrane currents were offline compensated for stimulus artefacts using Igor Pro 5.03 software. Ten traces evoked by 10 mV voltage steps from –80 to –70 mV were averaged and fitted mono-exponentially. Compensated current traces were obtained by multiplying the fitted curve by the respective factors and subsequent subtraction from the original current traces at different membrane potentials. Evoked glial PSCs (ePSCs) were compensated for stimulus artefacts by subtracting averaged failure traces.

Cell identification and immunohistochemistry

In this study, weakly fluorescent glial cells of the GluR type have been investigated, the properties of which have been reported in detail elsewhere (Matthias et al., 2003; Wallraff et al., 2004). For morphological and immunohistochemical analysis, the recorded cells were labelled by adding a red fluorescent dye (0.1% dextran-conjugated Texas Red or 0.1% dextran-conjugated TRITC, MW 3000, Molecular Probes, Leiden, Netherlands) to the pipette solution. Slices were fixed overnight with 8% paraformaldehyde in 0.1 M phosphate buffered saline (PBS) at 4°C. NG2 and S100β immunoreactivity was tested through double labelling using immunofluorescent antibodies. After washing in Triton X-100 containing PBS, the tissue was incubated for 24 hours at 4°C with either a polyclonal rabbit antibody directed against S100β (Swant, Bellinzona, Switzerland; 1:500), or a polyclonal rabbit antibody directed against NG2 (gift of W.P. Stallcup; 1:500). After repeated rinsing in PBS, the slices were further incubated with goat anti-rabbit immunoglobulins coupled to biotin (Dianova; 1:200) and visualized with the streptavidin-conjugated fluorochrome, indocarbocyanine (Cy5, Dianova; 1:200). The sections were mounted on slides using immunofluore mounting medium (Confocal-Matrix, micro-tech-lab, Graz, Austria) and evaluated using a confocal laser-scanning microscope in an inverted configuration (Leica TCS 4D, Leica, Bensheim, Germany). To avoid crossover of fluorescence between channels, sequential scanning was used with tight filter bands centred on the peak emissions of EGFP, TRITC and CY5. Cell morphology was visualized by taking consecutive optical sections up to a depth of 40 μm. Each channel was projected into a 2D micrograph using maximum intensity projection. The three greyscale pictures were combined by assigning them to the pseudo red (CY5), blue (EGFP), and green (Texas Red or TRITC) channels of an RGB picture. Immunoreactivity and the size of the cells were estimated using Metaview 4.5 software (Universal Imaging Corp., Downingtown, PA, USA). Therefore, background corrected 8 bit greyscale values of the tracer-filled cells were averaged and compared with the fluorescence intensity of adjacent immunopositive cells. The size covered by cell processes was measured as area. Reagents were purchased from Sigma unless otherwise stated. Data are given as mean ±s.d. Differences were tested for significance using the Student's *t*-test (P<0.05).

Results

Synapse-like structures can be found between neurons and glial cells with hGFAP promoter activity

To search for synapse-like structures between neurons and glial cells, we used hGFAP/EGFP transgenic mice, immunolabelled glial compartments with an antibody against GFP and studied sections on the ultrastructural level. Three approaches were used to detect the antibody: pre-embedding incubation of the antibody and visualization by either the DAB reaction or silver enhancement and post-embedding labelling by gold particles. The former techniques (DAB reaction and silver enhancement) had the advantage of better tissue preservation, but fine structures within the glial cytoplasm could not be recognized. Conversely, the post-embedding labelling had a poorer tissue preservation, but it was possible to recognize postsynaptic densities and endoplasmic reticulum within the glial compartment. Neuronal elements containing vesicles apposed to EGFP-positive glial compartments were detected with all techniques applied. The neuronal elements had the typical features of presynaptic terminals (Peters and Palay, 1996). With the pre-embedding technique, glial compartments were clearly labelled and could be easily identified (Fig. 1A,B). With the post-embedding technique, the gold particles were quantified to identify EGFP-positive compartments. We found postsynaptic density-like structures within glial compartments apposed to presynaptic-like specializations including the presence of vesicles (Fig. 1C,D). An accumulation of vesicles in EGFP-positive compartments adjacent to non-labelled (neuronal) structures was never observed. Two types of hGFAP/EGFP-positive cells were found to co-exist in the hippocampus, termed GluR and Glu-T cells (Matthias et al., 2003). Vesicles competent for regulated exocytosis were recently localized to one of these cell populations, the GluT cells (or 'passive' astrocytes; Bezzi et al., 2004). The ultrastructural methods applied here did not allow us to distinguish between EGFP-positive GluR and GluT cells. However, the absence of vesicles in the glial compartments suggested that processes of GluR cells, rather than GluT cells, form specialized junctions with presynaptic terminals to receive synaptic input from neurons.

Identification of GluR cells receiving synaptic input through post-recording immunhistochemistry

Patch clamp recordings were performed to test for synaptic innervation of the two types of hGFAP/EGFP-positive cells, and subsequent post-recording immunocytochemistry was employed to confirm cell type identification. As explained later in detail, only GluR cells received synaptic input. Typical properties of such a weakly EGFP-positive GluR cell with synaptic input from neurons are shown in Fig. $2A_1$. In addition to their 'complex' current pattern (Fig. $2A_1$ middle) cf. (Steinhäuser et al., 1994), these cells are characterized by an extended net of thin processes surrounding the soma as revealed through intracellular labelling (Fig. $2A_1$ left). The processes characteristically displayed small nodules and covered an area of 3445±2010 μm^2 (*n*=6). All GluR cells tested expressed the proteoglycan, NG2 (6/6 cells; Fig. $2A_1$ right). As in adult mice (Wallraff et al., 2004), these cells never displayed dye coupling and did not contact blood vessels. Hence, GluR cells were easily distinguishable from GluT cells, which display different functional and morphological properties (Fig. $2A_2$). The processes of the GluT cells ramified from a few thick branches down to a fine sponge-like network (Hama et al., 2004), which could not be resolved with confocal microscopy and appears 'foggy' in the picture (Fig. A_2, B_3, left). The areas covered by processes (2209±240 μm^2, *n*=3) did not differ from those of GluR cells. All GluT cells tested were NG2 negative (3/3 cells) (Fig. $2A_2$, right). Both cell types were tested for the expression of S100β (Fig. $2B_{1\text{-}3}$). To reduce potential washout

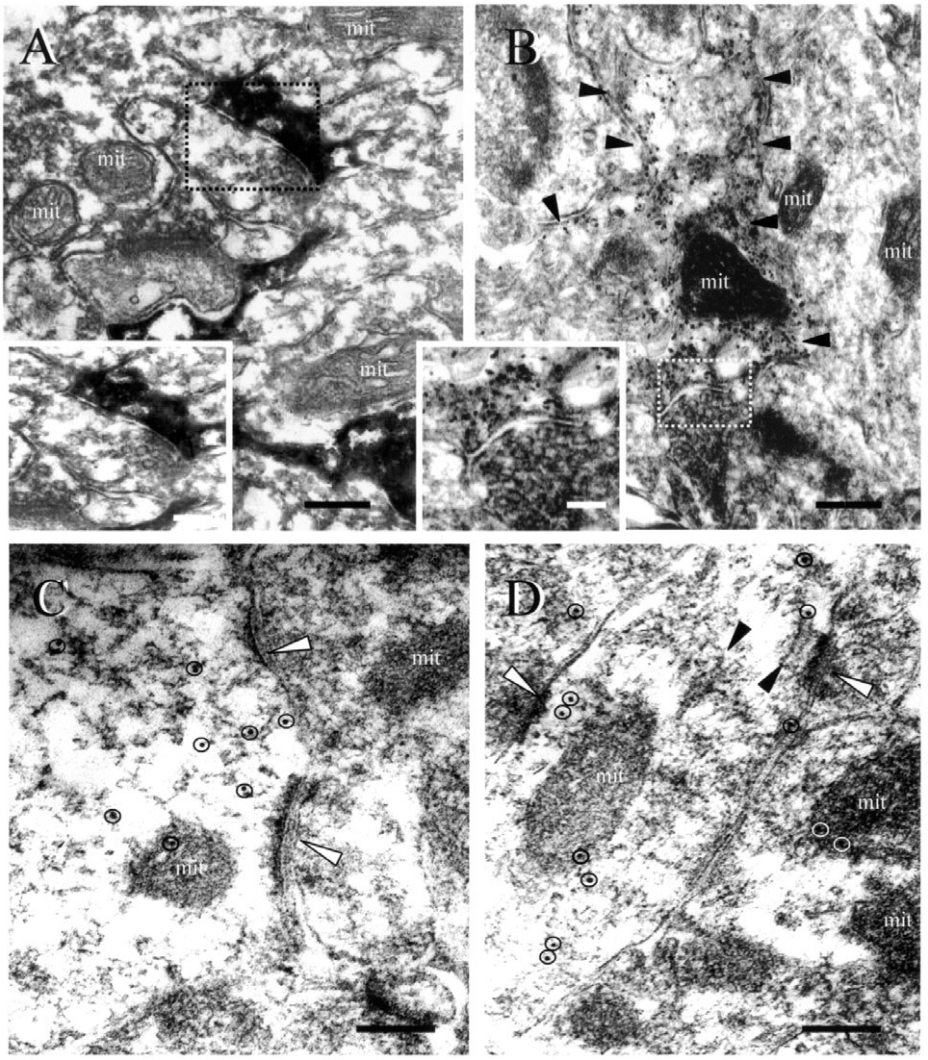

Fig. 1. Morphological evidence of synapse-like structures between hGFAP/EGFP-positive glial cells and neurons. Glial cells in the hippocampal CA1 area of hGFAP/EGFP transgenic mice were immunolabelled by anti-GFP antibodies and visualized by HRP-reaction (A), silver intensified immunogold reaction (B) and post-embedding labelling with immunogold particles (C,D). EGFP-positive profiles in A are visible by dense, black peroxidase reaction product. In B, glial profiles (outlined by arrowheads) are labelled by black silver grains. EGFP-positive presumed GluR cells in A and B are in contact with synaptic nerve terminals. Areas of glial-neuron contact are magnified in the inserts (delineated by dashed rectangles). Scale bar in A, B=0.2 μm and 0.1 μm in inserts. Synapse-like structures in (C,D) display typical synaptic terminals with synaptic vesicles inside the neuronal 'partner' and post-synaptic densities (arrowheads) in the labelled EGFP-positive glial profiles. Circles are intended to mark the 12 nm gold particles. There are also mitochondria (mit) and endoplasmic reticulum (black arrow head) in the labelled profiles. Note unspecific gold labelling on mitochondria in (C,D). Scale bars in C,D=0.25 μm.

of cytosolic proteins through the patch pipette, recording time was limited to exactly 1 min. Seven out of 10 GluT cells and 5 out of 15 GluR cells were S100β-positive. In some cells, immunoreactivity was consecutively quantified to estimate the possible effect of washout (cf. Materials and Methods). The series resistance and the cell volume were estimated for cells stained against S100β, since these parameter mainly determine the time constant of equilibration of a substance in the whole cell configuration (Pusch and Neher, 1988; Müller et al., 2005). There was no significant difference between S100β-positive (n=6) and S100β-negative (n=9) cells with respect to these parameters. The presence of GFAP mRNA together with the post-recording S100β immunoreactivity in 30% of the GluR cells indicates that the cells analysed here represent an intermediate cell type rather than OPCs as suggested by work of Bergles and colleagues (Bergles et al., 2000; Lin and Bergles, 2003).

Sub-threshold stimulation of Schaffer collaterals and simultaneous current-clamp recording revealed synaptic innervation of GluR-type glial cells

To test whether GluR cells receive synaptic input, stimulation pulses were applied through a bipolar platinum wire electrode located in the Schaffer collaterals, and a glial cell was analysed with the patch-clamp method. Simultaneously, field potentials were monitored in the stratum radiatum with an electrode placed in the close vicinity (20-40 μm) of the recorded cell. Since evoked field potentials are not spatially homogenous over large areas, this approach allowed a controlled fine-tuning of the excitation level evoked in the tissue surrounding the analysed glial cell. To avoid the generation of postsynaptic action potentials and recurrent neuronal circuits, stimulation intensity was adjusted sub-threshold (50-150 microseconds, 50-250 pA, 120 stimuli at 1 second intervals). The presence of afferent fiber volleys and dendritic field potentials verified successful fibre tract stimulation and presynaptic transmitter release (Fig. $3B_1$). Under these conditions, current clamp recordings revealed stimulus-correlated depolarizations of the glial cell membrane (n=12/19 cells) (Fig. $3A_1$). Repetitive stimulation at constant intensity evoked postsynaptic potentials in GluR cells (ePSPs) of up to 8 mV, but also disclosed a significant failure rate (Fig. $3A_2$,C,D_1). Analysis of amplitude histograms revealed a Gaussian distribution of baseline fluctuation of the glial membrane potential (Fig. $3D_2$), but the glial ePSPs were clearly non-Gaussian distributed (Fig. $3D_1$). This observation suggested quantal transmitter release at a neuron-glia synapse-like structure and predicted the existence

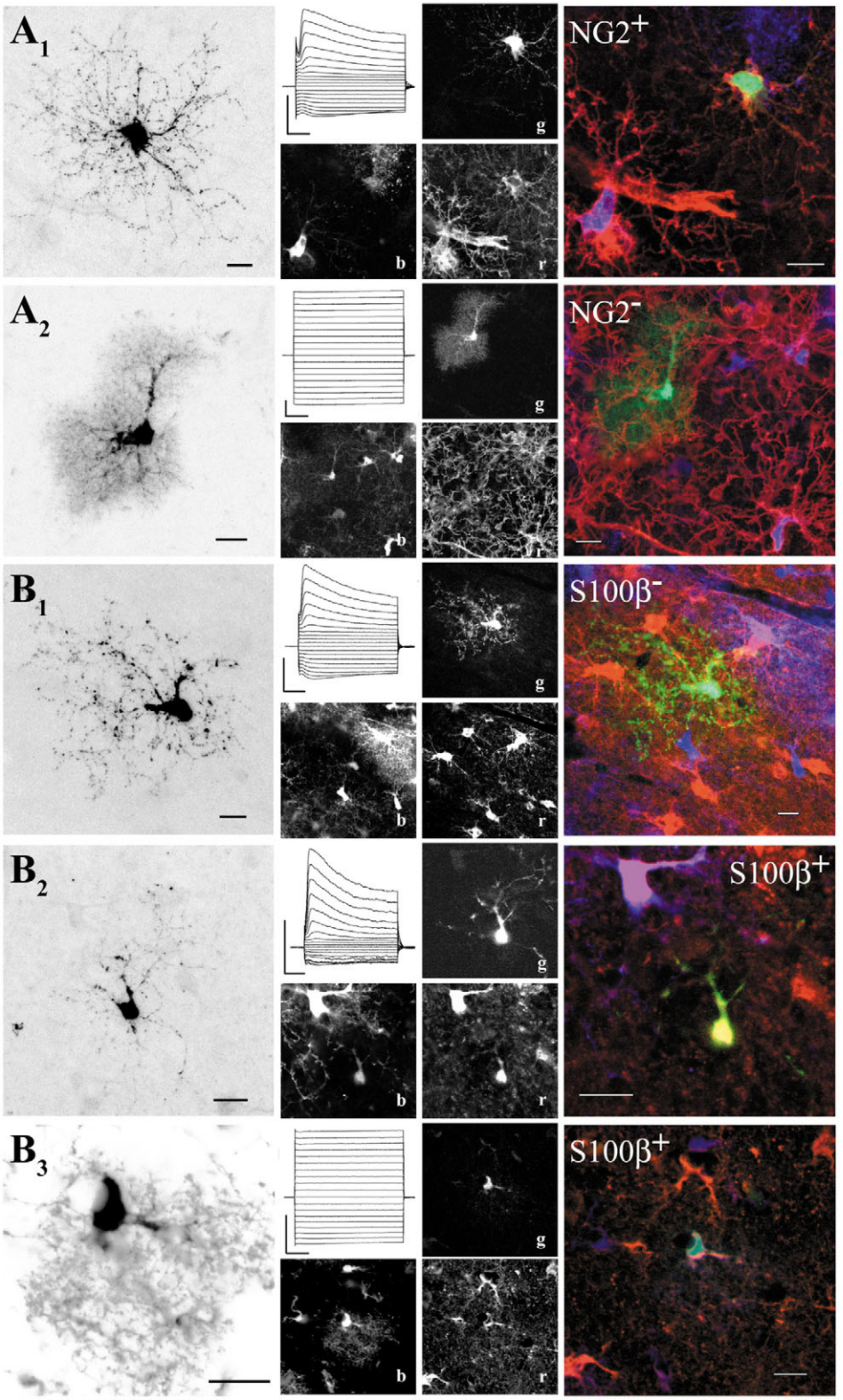

Fig. 2. Post-recording analysis of hGFAP/EGFP-positive cells in the hippocampus. (A_1) The morphology of a GluR cell was visualized by Texas Red dextran-filling during whole cell recording. Subsequent confocal analysis and 2D projection of 32 optical sections (total depth 21 μm) allowed us to resolve details of cellular process arborization. Note the typical nodules appearing as dots all along the fine processes. The current pattern of this GluR-type glial cell is given in the middle panel. Current responses were evoked by de- and hyperpolarizing the membrane between +20 and –160 mV (holding potential –80 mV), and capacitive artefacts were compensated offline (V_{rest}=–83 mV, R_i=78 MΩ, C_m=37 pF). This cell showed sPSPs and ePSPs sensitive to NBQX and bicuculline. Post-recording immunostaining and triple fluorescence confocal analysis were applied to check for NG2 immunoreactivity. The middle panel shows the three separated colour channels of one confocal plane. To improve visibility, Texas Red dextran labelling of the recorded cell is given in green (g), NG2 immunoreactivity in red (r), and EGFP expression in blue (b). Note that the EGFP fluorescence remaining post-recording was only 16% compared to surrounding cells (b). The superimposed RGB picture (right panel) shows the membrane-associated distribution of NG2 immunoreactivity of the recorded GluR cell (yellow details). (A_2) In contrast to GluR cells, hGFAP/EGFP-positive GluT type astrocytes predominantly expressed time- and voltage-independent currents (middle panel, stimulus protocol as in A_1) and displayed a different morphology (left panel, see text for details; V_{rest}=–84 mV, R_i=3 MΩ, C_m=71 pF). The cell did not generate sPSCs. The EGFP fluorescence intensity determined post-recording reached 53% of that measured in adjacent cells (b). The cell was NG2-negative (middle panel (r) and right panel). (B_{1-3}) Analogue to (A), GluR and GluT cells were tested post-recording for S100β immunoreactivity. The cells were recorded for exactly 1 minute (see text). (B_1, left) 2D projection of a GluR cell after TRITC dextran-filling (16 optical sections, total depth 8.4 μm) revealed a typical morphology with thin, wide spanning, nodule-containing processes. (B_1, middle) Artefact-compensated current pattern of the GluR cell (V_{rest}=–84 mV, R_i=72 MΩ, C_m=29 pF). In this cell, post-recording analysis did not detect S100β immunoreactivity [S100β, red (r); TRITC dextran, green (g)]. (B_2) Another GluR cell (V_{rest}=–83 mV, R_i=270 MΩ, C_m=24 pF) showed post-recording S100β labelling. (B_3) Analysis of a GluT cell. Projection of EGFP fluorescence (left, 32 optical sections, total depth 19.5 μm) revealed its characteristic morphology. (B_3, middle) Current pattern of the GluT cell (V_{rest}=–86 mV, R_i=5.1 MΩ, C_m=61 pF). The cell was filled with Texas Red dextran (g) during recording, and post-recording confocal analysis detected S100β immunoreactivity [71% fluorescence intensity compared with surrounding S100β-positive cells (r)]. Scale bars in morphological pictures represent 10 μm; for current patterns, 1 nA and 10 milliseconds, respectively.

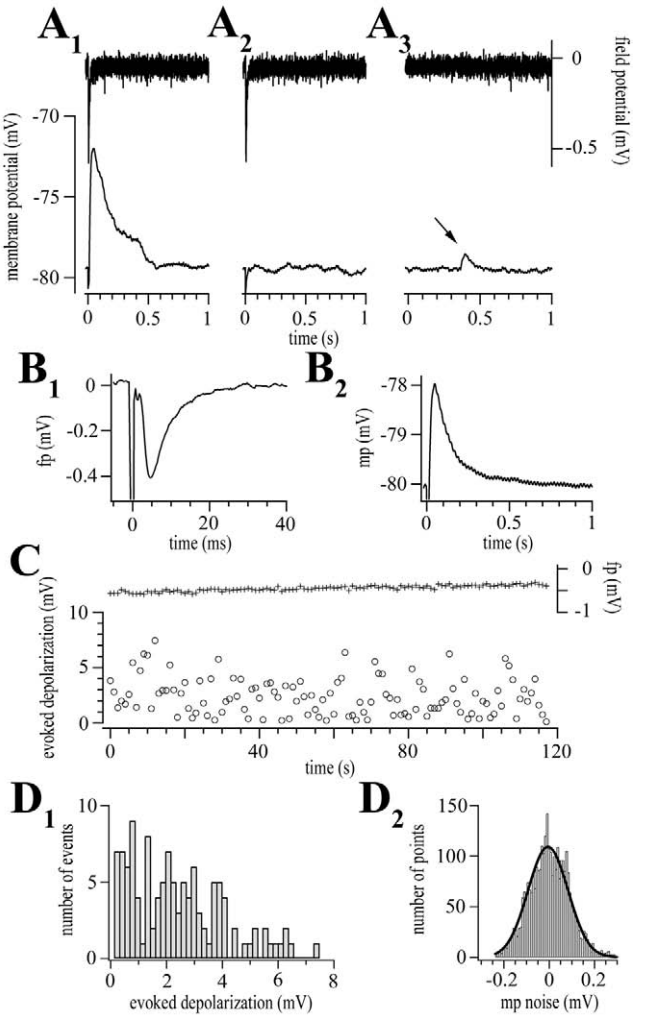

Fig. 3. Repetitive sub-threshold Schaffer-collateral stimulation (100 microseconds, 1 Hz) revealed postsynaptic depolarisations of unequally distributed amplitudes in GluR-type glial cells. Extracellular field potentials and membrane potentials of a GluR cell were simultaneously recorded in a p11 mouse (V_{rest}=–80 mV, R_i=400 MΩ, C_m=30 pF). (A) Typical pairs of recording traces are given. Single stimulation pulses caused stable dendritic field potentials ($A_{1,2}$ upper traces, C upper trace) and time-correlated glial depolarizations of up to 7.3 mV (A_1, lower trace) or glial failures (A_2, lower trace). Spontaneous glial depolarisations were observed in a few cases (A_3 arrow, 0.9 mV). (B) The average of 119 successively recorded pairs of traces is depicted with different time scaling. (B_1) Field potentials showed only synaptic potentials (449±65 μV) without postsynaptic population spikes, as visualized at higher time resolution. (B_2) The corresponding glial ePSPs averaged out at 2.4±1.8 mV. (C) The time course of field potential amplitudes (crosses, upper trace) and GluR cell ePSPs is plotted. While field potentials remained almost unchanged, the glial responses represented a mixture of failures and depolarisations over the 2 minutes recording period (circles, lower panel). (D) The amplitudes of the glial ePSPs were clearly non-Gaussian distributed (D_1). The noise amplitude histogram was received from analysing baseline recorded at resting potential (1 second, corresponding to 3106 points) and fitting to a Gaussian function (D_2). The Gaussian fit displayed a half width of 124±5 μV and peaked at –80.7±0.09 mV. For clarity, the centre was scaled to 0 mV. All data in this figure were obtained from the same GluR cell, $[Cl^-]_i$ was always 135 mM.

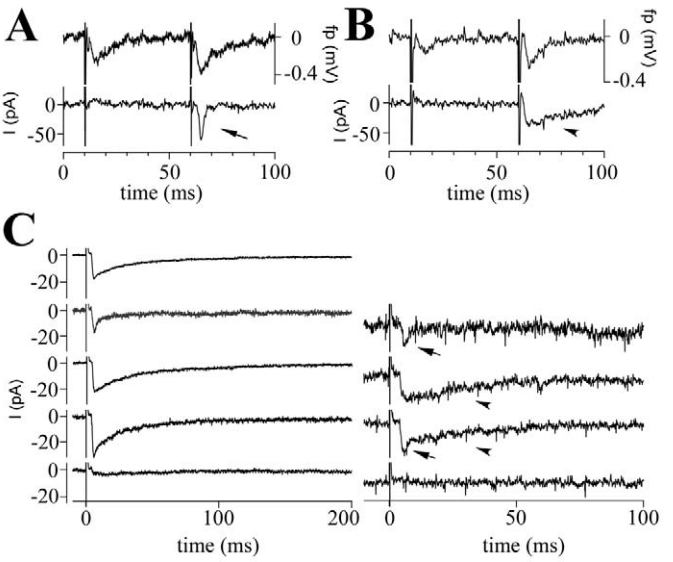

Fig. 4. Schaffer-collateral stimulation reveals two types of glial ePSCs with different inactivation kinetics. (A,B) Sub-threshold field potentials (top traces) were elicited applying a paired pulse protocol (150 microseconds, 150 μA, 50 milliseconds interval, every 20 seconds) while recording a GluR cell in the voltage-clamp mode (–80 mV, bottom traces). Typical examples of rapidly (A, τ=2.4 milliseconds, arrow) and slowly (B, τ=33 milliseconds, arrowhead) inactivating glial ePSCs are shown. (C) Fast and slowly decaying ePSCs occurred in the same individual GluR cell. 120 single sub-threshold pulses (100 microseconds, 150 μA) were applied every 3 seconds while currents were recorded at –80 mV. The top left trace represents the total average of all responses. Subsequently, current traces were sorted according to inactivation time constants. The left panel shows averages of pooled responses, while the right panel gives typical original traces. The upper pair of traces shows fast inactivating currents (τ_{fast}=3.4 milliseconds, n=16), the next summarizes traces with slowly inactivating currents (t_{slow}=34.7 milliseconds, n=48), followed by responses with biphasic inactivation (τ_{fast}=4.6 milliseconds, τ_{slow}=30.3 milliseconds, n=16). The bottom pair shows failure traces (n=35). Arrows denote fast responses, arrowheads denote slowly decaying responses. $[Cl^-]_i$ was always 135 mM.

of spontaneous glial PSPs. Indeed, low-frequency, spontaneous PSPs (sPSPs) (Fig. 3A_3, bottom) occurred in most GluR cells tested (20/24).

By contrast, we never recorded ePSPs in GluT cells upon sub-threshold stimulation (16/16 cells). This might be due to their low input resistance (6.5 MΩ±4.4, n=16 versus 115±108 MΩ, n=24 for GluR cells), or indicate lack of synaptic innervation. Non-physiological, high-frequency stimulation (100 Hz for 1 second) was required to depolarize GluT cells (range 3-23 mV, mean 13.6 mV±5.3, n=11) (see also Fig. S1 in supplementary material), presumably reflecting elevation of the extracellular potassium concentration. Together, these data suggested that under physiological conditions GluR cells, but not GluT cells, are depolarised upon synaptic input from neurons.

Pharmacological analysis indicated monosynaptic GABAergic input onto GluR cells

Next we set out to identify the mechanism(s) underlying the

Table 1. Comparison of spontaneous and evoked PSCs of GluR cells

	aCSF	+ bicuculline (10 μM)	+ NBQX (10 μM) + APV (25 μM)
Fast spontaneous PSCs amplitude	6.7±2.4 pA (*n*=18)	4.8±0.7 pA (*n*=4)	
Fast evoked PSCs amplitude		3.8±1.2 pA (*n*=6)	
Slow spontaneous PSCs amplitude	6.2±2.0 pA (*n*=16)		5.0±1.9 pA (*n*=9)
Slow evoked PSCs amplitude			4.7±1.5 pA (*n*=7)
Fast spontaneous PSCs decay time constant	2.6±1.2 milliseconds (*n*=18)	2.7±0.8 milliseconds (*n*=4)	
Fast evoked PSCs decay time constant		1.9±1.2 milliseconds (*n*=6)	
Slow spontaneous PSCs decay time constant	16.0±7.4 milliseconds (*n*=16)		20±12 milliseconds (*n*=9)
Slow evoked PSCs decay time constant			25.4±7.2 milliseconds (*n*=7)
Fast spontaneous PSCs frequency	3.8±4.0 events per minute (*n*=18)	3.1±3.0 events per minute (*n*=4)	
Slow spontaneous PSCs frequency	1.0±0.7 event per minute (*n*=16)		1.0±0.5 event per minute (*n*=9)

None of the corresponding differences reached the level of statistical significance.

depolarisation of GluR cells. Voltage clamp recordings unravelled fast- and slow-decay time constants of the evoked responses, and both components were generated by individual GluR cells (*n*=14). Typical examples of fast and slow glial ePSCs are given in Fig. 4A,B. Both components were activated within about 1 millisecond in a stimulus-correlated manner and displayed decay time constants of 1-5 milliseconds and about 20 milliseconds, respectively. Occasionally, we also noted responses with two decay time constants (Fig. 4C). As expected for synaptic events, spontaneous glial PSCs (sPSCs) were also observed. Individual GluR cells displayed fast, slow, or biphasic sPSC kinetics; see below (Fig. 8A$_2$) (Table 1).

The identity of evoked (120 single stimulation pulses, interstimulus interval 3 seconds or 10 seconds) and spontaneous PSCs in GluR cells was investigated in the presence of antagonists of ionotropic glutamate and GABA$_A$ receptors. Application of NBQX (10 μM) completely abolished dendritic field potentials while the presynaptic fiber volley was still visible (Fig. 5A top panel). In the presence of this antagonist, slowly decaying glial ePSCs remained largely unchanged (*n*=3) (Fig. 5A lower panel). This indicated that (1) GluR cells received monosynaptic input and (2) a significant proportion of glial ePSCs were caused by receptors other than AMPA/kainate receptors. Application of bicuculline (10 μM) significantly and reversibly blocked the slow glial responses (*n*=4; Fig. 5B) while field potentials and fast, bicuculline-insensitive GluR cell ePSCs remained under these conditions (see below). These findings demonstrated that the slow responses were mediated by postsynaptic glial GABA$_A$ receptors.

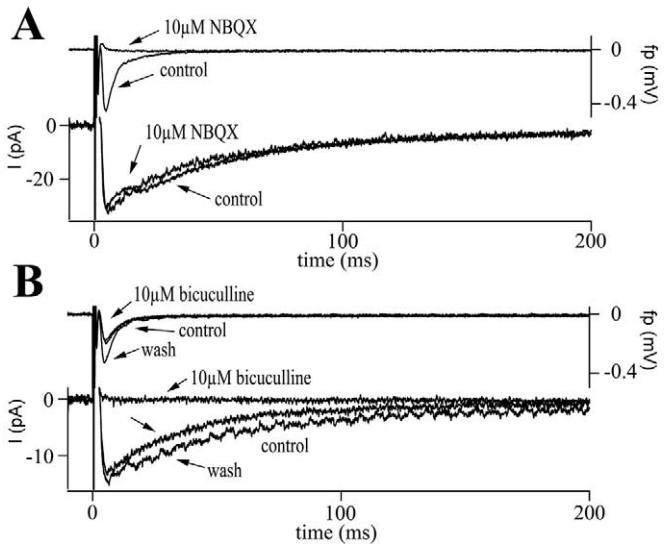

Fig. 5. Pharmacological identification of GABA$_A$ receptor-mediated ePSCs in GluR cells. (A,B) Averaged sub-threshold field potentials (top traces) and whole-cell currents (–80 mV, bottom) are depicted, which were recorded in response to 120 single stimulation pulses (150 μs, 10 second intervals) in the presence of NBQX (10 μM; A) or bicuculline (10 μM; B). Note the almost complete block of glial inward currents by bicuculline. $[Cl^-]_i$ was always 135 mM.

To investigate further the properties of GABA$_A$ receptor mediated glial ePSCs, interneurons were activated more directly through near field stimulation, and the Cl^- concentration of the patch pipette solution was reduced to 27 mM to mimic physiological conditions. In the presence of NBQX (10 μM) and APV (25 μM D-APV or 50 μM DL-APV), ePSCs of GluR cells displayed a mean amplitude of 4.7±1.5 pA and decayed with a time constant of 25.4±7.2 milliseconds (–80 mV, *n*=7). The failure rate was 69±15% (*n*=7) (Fig. 6B). The GABA mediated ePSCs could be completely blocked by 1 μM TTX (not shown). Reversal potential analysis was performed to confirm that the evoked glial responses were not due to GABA uptake. As a comparison, we first studied CA1 interneurons. Under our experimental conditions, GABA$_A$ receptor mediated spontaneous inhibitory postsynaptic currents (sIPSCs) recorded from CA1 neurons in the whole cell configuration reversed at –40 mV, which was close to the theoretical Cl^- equilibrium potential (E_{Cl^-}=–39.7 mV). Accordingly, changing the driving force for Cl^- in GluR cells by shifting the holding potential from –80 to 0 mV, led to outwardly directed glial ePSCs (Fig. 6C). Amplitudes amounted to 5.1±2.4 pA (*n*=4), which did not differ significantly from the absolute value measured at –80 mV (cf. above). These findings corroborated the view that the glial ePSCs were due to Cl^- passing through GABA$_A$ receptors.

In addition, sPSCs were registered in GluR cells in the presence of NBQX and APV (9/10 cells; Fig. 6D-G), which did not differ in amplitude (5.0±1.9 pA, *n*=9) and decay time (20±12 milliseconds, *n*=9) from the ePSCs described above. In contrast to neuronal sIPSCs (Banks et al., 2002; Mody and Pearce, 2004), the glial GABA mediated sPSCs occurred at very low frequencies (1.0±0.5 events per minute, *n*=9; Fig. 6D). To verify that these rare sPSCs did not represent irregular noise, sPSCs were provoked through depolarisation of

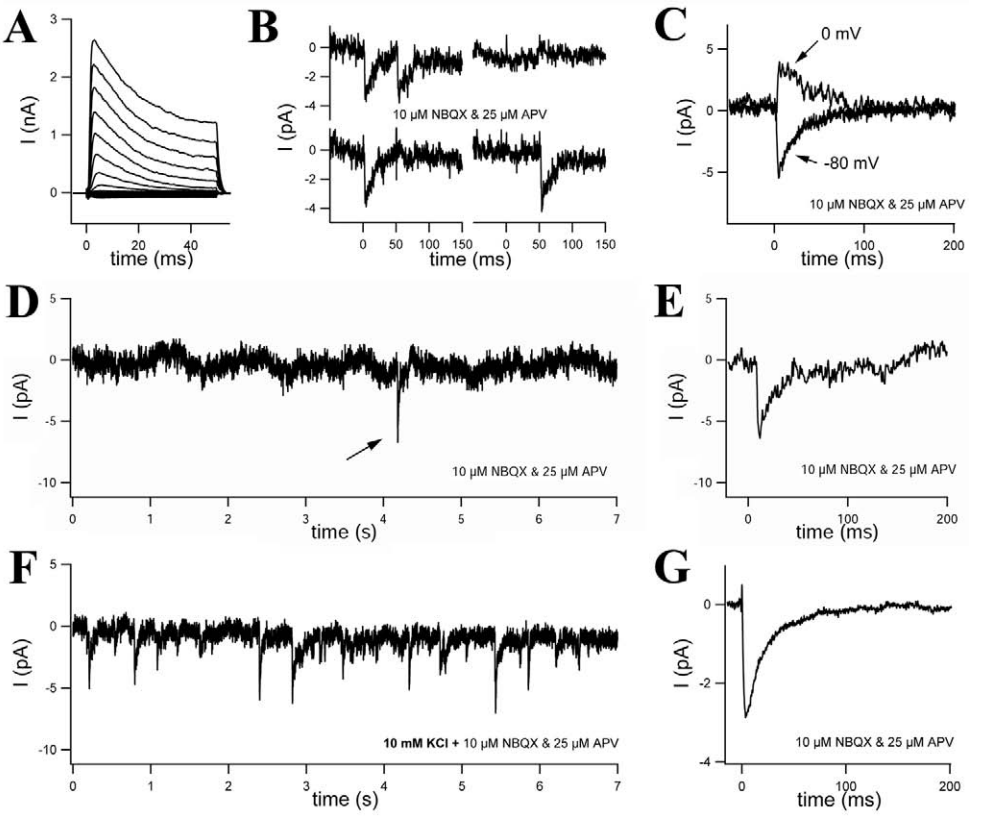

Fig. 6. Properties of postsynaptic $GABA_A$ receptor currents in hippocampal GluR cells. Data were taken in the presence of NBQX (10 μM) and D-APV (25 μM). (A) Membrane currents were evoked as described in Fig. 2A. (B) Paired-pulse stimulation (150 μs, 29 V, 50 milliseconds delay, 10 seconds interstimulus interval; 37 double pulses) evoked slowly decaying PSCs (τ~17 milliseconds). Currents were sorted according to stimulation success, and averaged. In 8 cases, both pulses evoked glial PSCs (upper left trace; amplitudes 3.0 and 2.4 pA) while 14 paired pulses produced double failures (right, top). Seven stimulation pairs induced responses upon the first (left, bottom), another 8 upon the second pulse (right, bottom). The total failure rate was 58%. (C) Short (150 μs) stimulation pulses evoked glial PSCs, which had opposite directions at –80 mV and 0 mV (averaged responses of 120 and 30 single traces, respectively). (D) Spontaneous GABA-mediated PSCs occurred rarely (about 1 event per minute; arrow). (E) Kinetics of the GABA-mediated glial sPSC labelled by an arrow in (D) at higher time resolution. (F) Increasing $[K^+]_o$ to 10 mM significantly increased the frequency glial GABA sPSCs (50 events per minute). (G) Analysis of averaged sPSCs (187 events) revealed an amplitude of 3.2 pA, a desensitization time constant of 19.5 milliseconds, a rise time of 1.9 milliseconds (10-90% time to peak), and a half width of 14.6 milliseconds. With the exception of (B), all recordings in this figure were obtained from the same individual cell; $[Cl^-]_i$ was always 27 mM.

presynaptic terminals by raising $[K^+]_{out}$. As expected, bath application of 10 mM KCl in the presence of NBQX and APV reversibly increased the incidence of GABA-induced sPSCs (to 32±16 events per minute; amplitude, 3.5±0.7 pA; decay time constant, 18.3±0.9 milliseconds, n=2) (Fig. 6F). Together, these data confirmed that the slow glial PSCs were due to activation of $GABA_A$ receptors in the GluR cell membrane.

Quantal analysis suggests a small number of presynaptic release sites giving rise to GABA mediated ePSCs in GluR-type glial cells

The $GABA_A$ receptor mediated glial sPSCs occurred at very low frequencies, and the evoked responses were characterized by small amplitudes and high failure rates. These properties indicated a low grade of synaptic innervation compared with hippocampal neurons. To achieve more information about the quantal nature of presynaptic GABA release onto the postsynaptic GluR cell membrane, the amplitude distribution of $GABA_A$ receptor mediated ePSCs was studied through independent (i.e. interstimulus interval 10 seconds) single pulse stimulation (Fig. 7). ePSCs averaged out at 5 pA, with a rise time of 1.8 milliseconds (Fig. 7A). Individual amplitudes of a given cell varied between 0 and 18 pA (e.g. Fig. 7B,C, n=4). Since the putative unitary amplitude and current noise were expected to be of the same order of magnitude, amplitudes for each cell were determined by averaging individual ePSCs within a fixed time window of 1 millisecond. The windows were placed at ±0.5 milliseconds of the averaged peak time for each cell. This allowed estimation of the noise-related error, which was characterised by the width of the Gaussian distribution around 0 pA (Fig. 7B,D,E). In contrast to baseline noise (Fig. 7D, inset), the ePSC amplitude histograms displayed non-Gaussian, binomial-like distributions, indicative of small numbers of release sites producing GABA-mediated glial ePSCs (Fig. 7D). Rough estimation yielded unitary amplitudes of about 1.3 pA. However, the superposition of amplitude histograms (n=4) did not display clear multiples of an unitary amplitude (Fig. 7E), even though all individual cells showed failures and ePSCs of non-Gaussian distributed amplitudes. Possible reasons for this finding will be discussed later on.

The rapid GABA-independent responses in GluR cells were inhibited by NBQX

As mentioned above, a second type of GluR cell PSCs were characterized by fast decay time constants (lower trace in Fig. $8A_2$). The rapid sPSCs and ePSCs were further analysed in the presence of the $GABA_A$ receptor antagonist, bicuculline (10 μM), which completely blocked the slow component. Bicuculline-resistant sPSCs occurred in all GluR cells tested

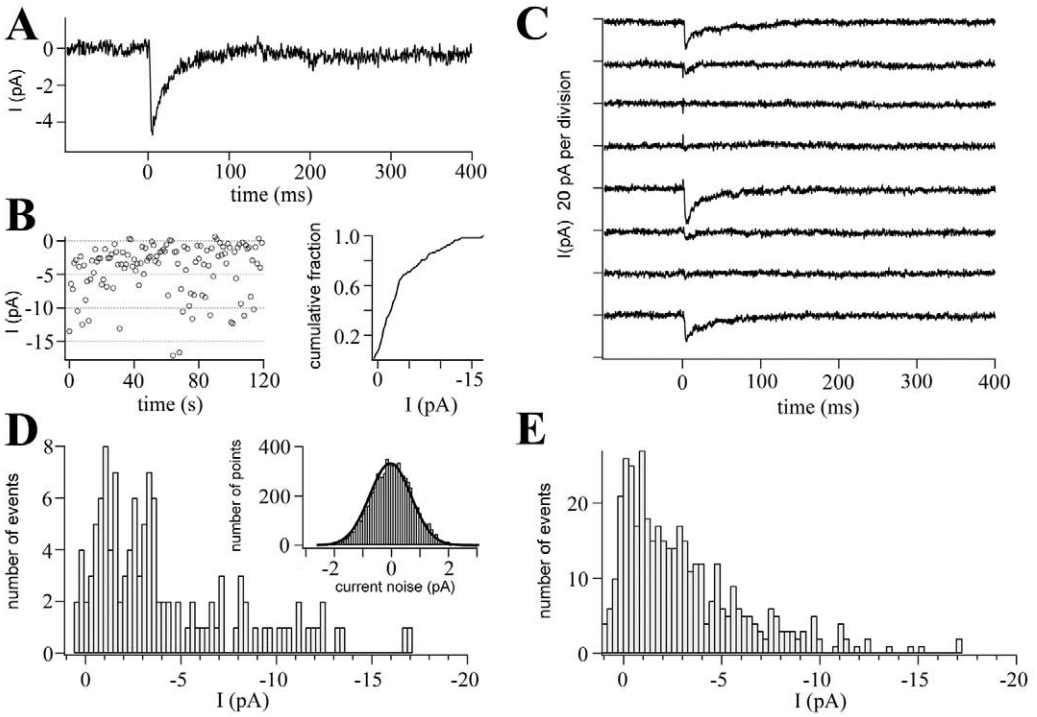

Fig. 7. Quantal analysis of GABA-mediated glial ePSCs suggests a small number of release sites. (A) Averaged response (120 stimuli, 150 microseconds) in the presence of NBQX (10 μM) and D-APV (25 μM). Peak amplitude (4.8 pA) was reached 5.4 milliseconds after the stimulus. (B) ePSC amplitudes were plotted against time (left), and the cumulative fraction was calculated (right). (C) Eight successively recorded exemplary traces document the presence of failures and ePSCs in GluR cells. (D) The ePSC amplitude histogram resembles a binomial distribution, characteristic of a small number of release sites. The individual ePSC amplitudes were determined as the difference between the averaged currents measured between 4.9 and 5.9 milliseconds after stimulation, and the average of 1 milliseconds corresponding baseline current. Inset depicts the amplitude histogram of current noise, taken from baseline traces before stimulation (–100 milliseconds to 0 milliseconds in C). Evaluation of 600 milliseconds baseline noise (7373 points) revealed a Gaussian distribution around 0 pA with a half width of 1.03 pA. (E) shows the superposition of ePSC amplitude histograms of 4 GluR cells (interstimulus interval, 10 seconds). $[Cl^-]_i$ was always 27 mM.

(*n*=4; 3.1±3.0 events per minute) (Fig. $8A_1$,A_3,A_4). They displayed amplitudes of 6.0±2.1 pA, decayed with a time constant of 2.7±0.7 milliseconds, and were blocked by co-application of bicuculline with D-APV (25 μM) and NBQX (10 μM; *n*=3) (Fig. $8A_5$).

In the presence of bicuculline, short (100-150 microseconds) stimulation pulses also evoked rapid inward currents in all GluR cells tested (*n*=6) (Fig. $8B_1$). The bicuculline-resistant glial ePSC amplitudes (3.8±1.2 pA) and decay time constants (1.9±0.4 milliseconds) did not differ from the spontaneous responses. The failure rate was 65±21%. Co-application of bicuculline with NBQX and D-APV abolished the responses (*n*=5) (Fig. $8B_2$). This data suggested that in addition to GABA-mediated responses, PSCs were also produced by presynaptic release of glutamate that activated AMPA receptors in the postsynaptic GluR cell membrane.

Analysis of spontaneous PSCs under unblocked conditions identifies GABA and glutamate as the predominating neurotransmitters at neuron-to-GluR cell synapses

The results presented so far demonstrated that the majority of GluR cells displayed postsynaptic currents (50/57 cells) and revealed the existence of two independent types of synaptic input onto the glial cells. To determine whether the glial cells receive synaptic input other than glutamatergic or GABAergic, control sPSCs (i.e. in the absence of receptor antagonists) were investigated in more detail. Therefore, sPSCs of 20 individual GluR cells were sorted out according to their decay kinetics, and the fast and slow components were compared with properties of the pharmacologically isolated AMPA/kainate and $GABA_A$ receptor-mediated sPSCs, respectively. Frequency of occurrence, amplitudes and decay time constants of the control events did not differ from those of the separated glutamate- and GABA-mediated sPSCs reported above (Table 1). Thus, it is rather unlikely that additional neurotransmitters substantially contributed to synaptic innervation of GluR cells.

Both types of sPSCs coexisted in the majority of cells tested (14/20). Two cells showed only GABA- and four cells only glutamtate-mediated sPSCs. Together, these results show that most GluR cells in the CA1 stratum radiatum are innervated by both GABAergic and glutamatergic neurons, with the latter producing sPSC at a higher frequency.

Discussion

We have previously identified a population of glial cells in the hippocampus, termed GluR cells, that are distinct from the classical types of glial cells, astrocytes, oligodendrocytes and microglia. These cells with hGFAP promoter activity displayed astroglial properties, but subsets of the GluR cells co-expressed

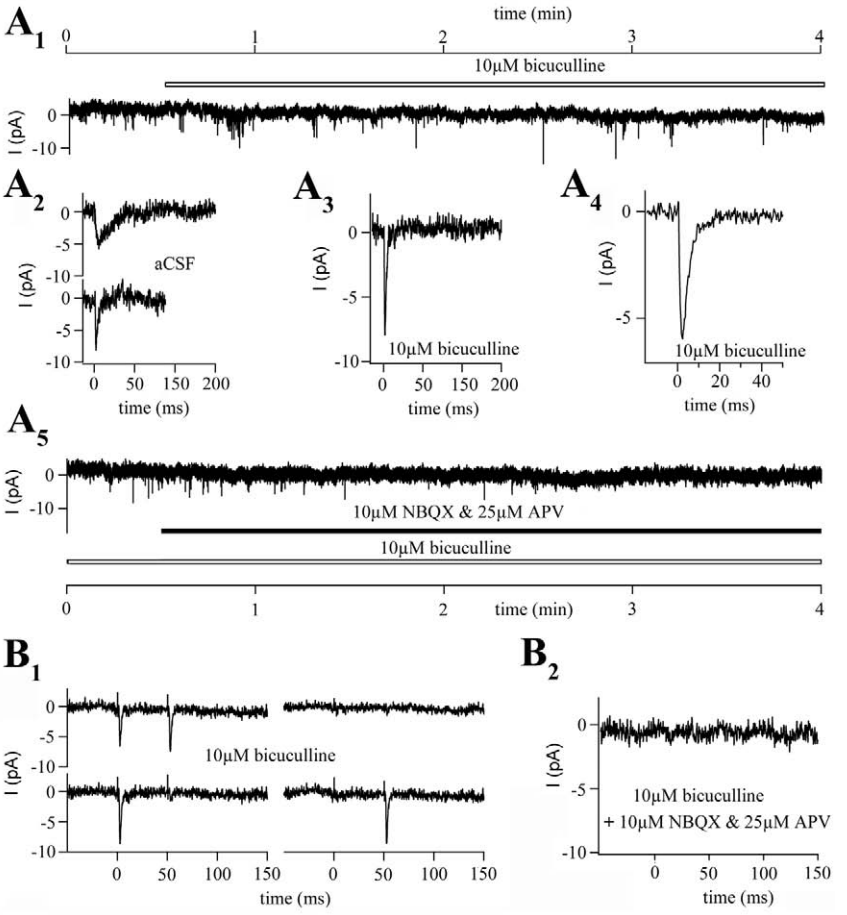

Fig. 8. GluR cells also receive glutamatergic input. Spontaneous (A_1-A_5) and evoked responses (B_1,B_2) were obtained from the same individual cell at p 10 (V_{rest}=–86 mV, R_i=230 MΩ, C_m=73 pF). (A_1-A_4) After application of bicuculline (10 μM), only the fast events persisted. (A_2) represents mean sPSCs with slow (top, 5.6 pA, τ=21.6 milliseconds, *n*=2) and rapid kinetics (bottom, 8.6 pA, τ=4.4 milliseconds, *n*=2) at higher resolution, taken from trace in (A_1) before bicuculline application (i.e. under control condition). The sPSC in (A_3) was taken from the trace in (A_1) during bicuculline application and displayed on a fast time scale and larger current scale. (A_4) shows the mean of 29 sPSCs taken from the trace in (A_1) during bicuculline at higher resolution [5.7±1.8 pA, τ=3.6 milliseconds, rise time 1.1 milliseconds (10-90%), half width 4.8 milliseconds]. (A_5) represents the continuation of the trace in bicuculline shown in (A_1), 15 minutes later. Note the presence of spontaneous, bicuculline-insensitive activity before and shortly after additional wash-in of NBQX (10 μM) and D-APV (25 μM). Two minutes after co-application of bicuculline with NBQX and APV, spontaneous activity completely disappeared. (B_1) In the same cell, near-field stimulation evoked bicuculline-resistant ePSCs with kinetics similar to the sPSCs (A_3,A_4). Paired pulses (*n*=119; 150 microseconds, 8V, 50 milliseconds delay, 1 second interstimulus interval) were applied, and currents were sorted and averaged as described in Fig. 6B. In 32 cases, both pulses evoked glial PSCs (upper left trace; amplitudes 6.7 and 6.9 pA; τ=1.5 milliseconds) while 29 paired pulses produced double failures (right, top). 21 stimulation pairs induced responses upon the first (left, bottom), another 37 upon the second pulse (right, bottom). The total failure rate was 49%. (B_2) Co-application of bicuculline with NBQX (10 μM) and D-APV (25 μM) led to a complete block of ePSCs. $[Cl^-]_i$ was always 27 mM.

the proteoglycan NG2 and transcripts for the neuronal glutamate transporter, EAAC1 (Matthias et al., 2003), and hence did not match the classical definition of an astrocyte (Kimelberg, 2004). Intriguingly, in the same brain region, NG2-positive cells were reported to receive direct synaptic input (Bergles et al., 2000; Lin and Bergles, 2003). While this seminal work added another level of complexity to CNS communication, the identity of the innervated glial cells remained a matter of debate because recent work from several laboratories questioned the usefulness of NG2 as an OPC marker (Nishiyama et al., 2002; Stallcup, 2002; Greenwood and Butt, 2003; Peters, 2004). We have found large numbers of GluR cells also in the adult and even aged hippocampus (Wallraff et al., 2004). This observation in conjunction with the low mitotic activity in the postnatal CA1 region (Rietze et al., 2000) make it very unlikely that a significant number of the NG2-positive GluR cells we have investigated in the juvenile hippocampus later on become oligodendrocytes. Here, we present first morphological and functional evidence of synaptic innervation of GluR cells. By quantitatively assessing amplitude distributions and failure rates of evoked postsynaptic glial responses, and by estimating the frequency of GABA versus glutamate-mediated inputs onto GluR cells, these data extend current knowledge of neuron-to-glia signalling mechanisms in the CNS.

Innervated GluR cells share properties of grey matter NG2 glia

To ascertain whether cells of the GluR type receive synaptic input, we recorded from cells in the hippocampal CA1 stratum radiatum displaying weak hGFAP-promoter activity as assessed by their low EGFP fluorescence intensity. Immunocytochemical and morphological analyses were performed subsequent to functional characterisation. All GluR cells tested expressed NG2, while about 30% of them were S100β-positive. Despite the reduced recording time, it can not be excluded that washout of the relatively small S100β molecule led to an underestimation of its expression. We noted that GluT cells, which represent ‘classical’ astrocytes in the hippocampus often displayed higher S100β immunoreactivity than GluR cells. The innervated GluR cells showed characteristic nodules, which occurred periodically along their processes. A similar morphology was described for so-called synantocytes, which are also NG2-positive (Berry et al., 2002).

For a long time NG2 was considered a marker of oligodendroglial precursor cells OPCs (Ong and Levine, 1999), but recent findings challenged this assumption (Butt, 2005). Ultrastructural (Nishiyama et al., 2002), immunohistochemical (Mallon et al., 2002; Matthias et al., 2003), and functional analyses (Chittajallu et al., 2004) in the cortex or hippocampus indicated that NG2 glia comprise a heterogeneous cell

population. Lineage analysis suggested that a subpopulation of postnatal NG2-positive cells in the early postnatal hippocampus represent neuronal progenitor cells (Belachew et al., 2003) while the coexpression of GFAP or vimentin with NG2 after lesion to the adult brain (Alonso, 2005) rather hints at an astroglial relationship of NG2 glia. Certainly, the cellular identity of these cells needs further consideration (Lin and Bergles, 2004).

Are all GluR cells innervated?

The infrequent incidence and the small amplitudes required long recording periods and low background noise to pinpoint sPSCs in the glial cells, and the success rate of ePSC activation additionally depended on appropriate positioning of the stimulation electrode. Considering these conditions, our data indicated that a majority of the GluR cells received both, GABA- and glutamate-mediated synaptic input. Whether the small group of cells apparently lacking PSCs represented a separate subpopulation of GluR cells or rather reflected inadequate recording conditions is difficult to decide. We noted that the input resistance of innervated GluR cells was variable, ranging between 80 to 1.500 MΩ (cf. Fig. S2 in supplementary material). However, it appeared that cells with lower values (R_i<20 MΩ) lacked both sPSCs and ePSCs. Further experiments are necessary to determine whether these cells comprise a distinctive subgroup of GluR cells devoid of synaptic input.

Are other neurotransmitters involved?

Expression of AMPA and $GABA_A$ receptors in GluR cells is well established (Jabs et al., 1994; Bekar et al., 1999; Zhou and Kimelberg, 2001; Matthias et al., 2003). Our data indicate that GluR cells receive only glutamatergic and GABAergic input: (1) The frequency of spontaneous events in control conditions matched the sum of activity either under blocked glutamate or $GABA_A$ receptor-mediated transmission; (2) sPSCs are completely absent when ionotropic GABA and glutamate receptors are blocked (Fig. $8A_5$). Similar types of neuron-to-glia synapses were also described for NG2-positive presumed OPCs (Bergles et al., 2000; Lin and Bergles, 2003). We cannot completely exclude that part of the fast decaying sPSCs in GluR cells was caused poly-synaptically, by the release of transmitter(s) other than GABA or glutamate. Indeed, astrocytes in the hippocampus were activated by neuronal release of noradrenaline or acetylcholine, which, however, stimulated metabotropic receptors in the glial membrane (reviewed by Fellin and Carmignoto, 2004; Volterra and Steinhäuser, 2004). Nicotinic acetylcholine receptors and glycine receptors have been found in glial subpopulations in situ or in the cell culture, but not in acute hippocampal slices (reviewed by Kettenmann and Steinhäuser, 2005). In conclusion, evidence available so far suggests that neuronal synaptic input onto GluR cells in the hippocampus activates postsynaptic AMPA and $GABA_A$ receptors only.

Properties of the neuron-glia signalling

A majority of the GluR cells received monosynaptic input from GABAergic neurons because in the case of polysynaptic circuits, block of glutamatergic transmission should have reduced sPSC frequency, which was not observed. Several reasons might account for the finding that quantal analysis of GABA-mediated glial ePSCs failed to reveal clear multiples of a unitary amplitude. First, the putative magnitude of the unitary current was in the range of 1 pA and therefore hardly to discriminate against current noise. However, reduction of noise due to superposition of histograms did not improve signal-to-noise relation. Therefore, a second explanation might be more appropriate. It is possible that GABA-mediated glial ePSCs have a varying quantal size, similar to neurons, where even single release sites show substantial variability (Ropert et al., 1990; Nusser et al., 2001). In the case of cultured hippocampal neurons, the quantal size variation of GABAergic synapses is mainly caused by the speed of GABA clearance from the synaptic cleft, while fluctuations of the initial peak concentration play only a minor role (Barberis et al., 2004). By contrast, ePSC kinetics remained unchanged in NG2-positive presumed OPCs after blockade of GABA transporters (Lin and Bergles, 2003). The reason for the smearing of the amplitude histograms of GluR cell ePSCs as observed here, still has to be elucidated.

Another question concerns the biphasic decay of the glial ePSCs (Fig. 4C), which might result from co-activation of postsynaptic AMPA and $GABA_A$ receptors, or represent an intrinsic property of the GABA-induced responses. Although a contribution of AMPA receptors cannot be completely excluded, the latter assumption appears more likely because biphasic PSCs also occurred spontaneously (n=3, not shown), a situation where the probability of simultaneous release of GABA and glutamate from two different fibers should be rather low. Moreover, biphasic ePSCs were also observed after inhibition of AMPA receptors. Whether the biphasic desensitisation kinetics hinted at prolonged concentrations of high GABA concentrations in the neuron-glia cleft, as observed for GABAergic neuronal communication (Celentano and Wong, 1994; Mozrzymas et al., 2003), remains to be investigated. Certainly, resolving the details of release mechanism and transmitter dynamics at GABAergic neuron-to-glia synapses represents a challenging task for future work.

Physiological role of neuron-to-GluR cell signalling

Astrocytes of the GluT type were shown to be in a position to release glutamate upon stimulation via regulated exocytosis (Bezzi et al., 2004), and to modulate the discharging pattern of neighbouring hippocampal neurons in situ (Fiacco and McCarthy, 2004; Liu et al., 2004; Angulo et al., 2004; Fellin et al., 2004, Volterra and Steinhäuser, 2004). However, our data do not suggest that GluT cells receive direct synaptic input. Whether GluR cells are capable of releasing transmitters upon neuronal stimulation is still unknown. The finding that GluR cells generated network driven, spontaneous membrane depolarisations hinted at a physiological role of the neuron-to-glia signalling. Although the glial PSDs measured at the somatic membrane were rather small, receptor activation at distant processes of GluR cells might interfere with other transmembrane proteins, e.g. Kir channels (Schröder et al., 2002) and lead to stronger, locally restricted depolarisations of subcellular microdomains, sufficient to activate intracellular signalling cascades. Future studies have to elucidate whether

the neuronal input is important for NG2-mediated clustering of AMPA receptors in GluR cells (Stegmüller et al., 2003) or is involved in more complex, e.g. growth factor-related glial reactions (Stallcup, 2002).

We gratefully acknowledge the excellent technical assistance of I. Krahner and wish to thank G. Laube (Institute of Anatomy, Charité, Berlin) for his help with low temperature embedding. This work was supported by grants of the Deutsche Forschungsgemeinschaft (JA942/2, SFB-TR3, KE 329/15-1), and Fonds der Chemischen Industrie (grant to C.S.).

References

Aguirre, A. A., Chittajallu, R., Belachew, S. and Gallo, V. (2004). NG2-expressing cells in the subventricular zone are type C-like cells and contribute to interneuron generation in the postnatal hippocampus. *J. Cell Biol.* **165**, 575-589.

Alonso, G. (2005). NG2 proteoglycan-expressing cells of the adult rat brain: Possible involvement in the formation of glial scar astrocytes following stab wound. *Glia* **49**, 318-338.

Angulo, M. C., Kozlov, A. S., Charpak, S. and Audinat, E. (2004). Glutamate released from glial cells synchronizes neuronal activity in the hippocampus. *J. Neurosci.* **24**, 6920-6927.

Banks, M. I., Hardie, J. B. and Pearce, R. A. (2002). Development of GABA(A) receptor-mediated inhibitory postsynaptic currents in hippocampus. *J. Neurophysiol.* **88**, 3097-3107.

Barberis, A., Petrini, E. M. and Cherubini, E. (2004). Presynaptic source of quantal size variability at GABAergic synapses in rat hippocampal neurons in culture. *Eur. J. Neurosci.* **20**, 1803-1810.

Baude, A., Nusser, Z., Roberts, J. D., Mulvihill, E., McIlhinney, R. A. and Somogyi, P. (1993). The metabotropic glutamate receptor (mGluR1 alpha) is concentrated at perisynaptic membrane of neuronal subpopulations as detected by immunogold reaction. *Neuron* **11**, 771-787.

Baude, A., Nusser, Z., Molnár, E., McIlhinney, R. A. J. and Somogyi, P. (1995). High-resolution immunogold localization of AMPA type glutamate receptor subunits at synaptic and non-synaptic sites in rat hippocampus. *Neuroscience* **69**, 1031-1055.

Bekar, L. K., Jabs, R. and Walz, W. (1999). $GABA_A$ receptor agonists modulate K^+ currents in adult hippocampal glial cells in situ. *Glia* **26**, 129-138.

Belachew, S., Chittajallu, R., Aguirre, A. A., Yuan, X., Kirby, M., Anderson, S. and Gallo, V. (2003). Postnatal NG2 proteoglycan-expressing progenitor cells are intrinsically multipotent and generate functional neurons. *J. Cell Biol.* **161**, 169-186.

Bergles, D. E., Roberts, J. D., Somogyi, P. and Jahr, C. E. (2000). Glutamatergic synapses on oligodendrocyte precursor cells in the hippocampus. *Nature* **405**, 187-191.

Berry, M., Hubbard, P. and Butt, A. M. (2002). Cytology and lineage of NG2-positive glia. *J. Neurocytol.* **31**, 457-467.

Bezzi, P., Gundersen, V., Galbete, J. L., Seifert, G., Steinhäuser, C., Pilati, E. and Volterra, A. (2004). Astrocytes contain a vesicular compartment that is competent for regulated exocytosis of glutamate. *Nat. Neurosci.* **7**, 613-620.

Butt, A. M. (2005). Structure and function of oligodendrocytes. In *Neuroglia.* 2nd edn (ed. H. Kettenmann and B. R. Ransom), pp. 36-47. Oxford: Oxford University Press.

Celentano, J. J. and Wong, R. K. (1994). Multiphasic desensitization of the GABAA receptor in outside-out patches. *Biophys. J.* **66**, 1039-1050.

Chittajallu, R., Aguirre, A. and Gallo, V. (2004). NG2-positive cells in the mouse white and grey matter display distinct physiological properties. *J. Physiol.* **561**, 109-122.

Fellin, T. and Carmignoto, G. (2004). Neurone-to-astrocyte signalling in the brain represents a distinct multifunctional unit. *J. Physiol.* **559**, 3-15.

Fellin, T., Pascual, O., Gobbo, S., Pozzan, T., Haydon, P. G. and Carmignoto, G. (2004). Neuronal synchrony mediated by astrocytic glutamate through activation of extrasynaptic NMDA receptors. *Neuron* **43**, 729-743.

Fiacco, T. A. and McCarthy, K. D. (2004). Intracellular astrocyte calcium waves in situ increase the frequency of spontaneous AMPA receptor currents in CA1 pyramidal neurons. *J. Neurosci.* **24**, 722-732.

Greenwood, K. and Butt, A. M. (2003). Evidence that perinatal and adult NG2-glia are not conventional oligodendrocyte progenitors and do not depend on axons for their survival. *Mol. Cell. Neurosci.* **23**, 544-558.

Hama, K., Arii, T., Katayama, E., Marton, M. and Ellisman, M. H. (2004). Tri-dimensional morphometric analysis of astrocytic processes with high voltage electron microscopy of thick Golgi preparations. *J. Neurocytol.* **33**, 277-285.

Haydon, P. G. (2001). GLIA: listening and talking to the synapse. *Nat. Rev. Neurosci.* **2**, 185-193.

Jabs, R., Kirchhoff, F., Kettenmann, H. and Steinhäuser, C. (1994). Kainate activates Ca^{2+}-permeable glutamate receptors and blocks voltage-gated K^+ currents in glial cells of mouse hippocampal slices. *Pflügers Arch.* **426**, 310-319.

Kettenmann, H. and Steinhäuser, C. (2005). Receptors for neurotransmitters and hormones. In *Neuroglia.* 2nd edn. (ed. H. Kettenmann and B. R. Ransom), pp. 131-145. Oxford: University Press.

Kimelberg, H. K. (2004). The problem of astrocyte identity. *Neurochem. Int.* **45**, 191-202.

Lin, S. C. and Bergles, D. E. (2003). Synaptic signaling between GABAergic interneurons and oligodendrocyte precursor cells in the hippocampus. *Nat. Neurosci.* **7**, 24-32.

Lin, S. C. and Bergles, D. E. (2004). Synaptic signaling between neurons and glia. *Glia* **47**, 290-298.

Liu, Q. S., Xu, Q., Arcuino, G., Kang, J. and Nedergaard, M. (2004). Astrocyte-mediated activation of neuronal kainate receptors. *Proc. Natl. Acad. Sci. USA* **101**, 3172-3177.

Mallon, B. S., Shick, H. E., Kidd, G. J. and Macklin, W. B. (2002). Proteolipid promoter activity distinguishes two populations of NG2-positive cells throughout neonatal cortical development. *J. Neurosci.* **22**, 876-885.

Matthias, K., Kirchhoff, F., Seifert, G., Hüttmann, K., Matyash, M. and Kettenmann, H. and Steinhäuser, C. (2003). Segregated expression of AMPA-type glutamate receptors and glutamate transporters defines distinct astrocyte populations in the mouse hippocampus. *J. Neurosci.* **23**, 1750-1758.

Mody, I. and Pearce, R. A. (2004). Diversity of inhibitory neurotransmission through $GABA_A$ receptors. *Trends Neurosci.* **27**, 569-575.

Mozrzymas, J. W., Barberis, A., Mercik, K. and Zarnowska, E. D. (2003). Binding sites, singly bound states, and conformation coupling shape GABA-evoked currents. *J. Neurophysiol.* **89**, 871-883.

Muller, A., Kukley, M., Stausberg, P., Beck, H., Müller, W. and Dietrich, D. (2005). Endogenous Ca^{2+} buffer concentration and Ca^{2+} microdomains in hippocampal neurons. *J. Neurosci.* **25**, 558-565.

Newman, E. A. (2003). New roles for astrocytes: Regulation of synaptic transmission. *Trends Neurosci.* **26**, 536-542.

Nishiyama, A., Watanabe, M., Yang, Z. and Bu, J. (2002). Identity, distribution, and development of polydendrocytes: NG2-expressing glial cells. *J. Neurocytol.* **31**, 437-455.

Nolte, C., Matyash, M., Pivneva, T., Schipke, C. G., Ohlemeyer, C., Hanisch, U. K., Kirchhoff, F. and Kettenmann, H. (2001). GFAP promoter-controlled EGFP-expressing transgenic mice: A tool to visualize astrocytes and astrogliosis in living brain tissue. *Glia* **33**, 72-86.

Nusser, Z., Cull-Candy, S. and Farrant, M. (1997). Differences in synaptic $GABA_A$ receptor number underlie variation in GABA mini amplitude. *Neuron* **19**, 697-709.

Nusser, Z., Naylor, D. and Mody, I. (2001). Synapse-specific contribution of the variation of transmitter concentration to the decay of inhibitory postsynaptic currents. *Biophys. J.* **80**, 1251-1261.

Ong, W. Y. and Levine, J. M. (1999). A light and electron microscopic study of NG2 chondroitin sulfate proteoglycan-positive oligodendrocyte precursor cells in the normal and kainate-lesioned rat hippocampus. *Neuroscience* **92**, 83-95.

Peters, A. (2004). A fourth type of neuroglial cell in the adult central nervous system. *J. Neurocytol.* **33**, 345-357.

Peters, A. and Palay, S. L. (1996). The morphology of synapses. *J. Neurocytol.* **25**, 687-700.

Pusch, M. and Neher, E. (1988). Rates of diffusional exchange between small cells and a measuring patch pipette. *Pflügers Arch.* **411**, 204-211.

Rietze, R., Poulin, P. and Weiss, S. (2000). Mitotically active cells that generate neurons and astrocytes are present in multiple regions of the adult mouse hippocampus. *J. Comp. Neurol.* **424**, 397-408.

Ropert, N., Miles, R. and Korn, H. (1990). Characteristics of miniature inhibitory postsynaptic currents in CA1 pyramidal neurones of rat hippocampus. *J. Physiol.* **428**, 707-722.

Schipke, C. G. and Kettenmann, H. (2004). Astrocyte responses to neuronal activity. *Glia* **47**, 226-232.

Schröder, W., Seifert, G., Hüttmann, K., Hinterkeuser, S. and Steinhäuser, C. (2002). AMPA receptor-mediated modulation of inward rectifier K^+ channels in astrocytes of mouse hippocampus. *Mol. Cell. Neurosci.* **19**, 447-458.

Stallcup, W. B. (2002). The NG2 proteoglycan: Past insights and future prospects. *J. Neurocytol.* **31**, 423-435.

Stegmüller, J., Werner, H., Nave, K. A. and Trotter, J. (2003). The proteoglycan NG2 is complexed with alpha-amino-3-hydroxy-5-methyl-4-isoxazolepropionic acid (AMPA) receptors by the PDZ glutamate receptor interaction protein (GRIP) in glial progenitor cells. Implications for glial-neuronal signaling. *J. Biol. Chem.* **278**, 3590-3598.

Steinhäuser, C., Jabs, R. and Kettenmann, H. (1994). Properties of GABA and glutamate responses in identified glial cells of the mouse hippocampal slice. *Hippocampus* **4**, 19-36.

Volterra, A. and Steinhäuser, C. (2004). Glial modulation of synaptic transmission in the hippocampus. *Glia* **47**, 249-257.

Wallraff, A., Odermatt, B., Willecke, K. and Steinhäuser, C. (2004). Distinct types of astroglial cells in the hippocampus differ in gap junction coupling. *Glia* **48**, 36-43.

Zhou, M. and Kimelberg, H. K. (2001). Freshly isolated hippocampal CA1 astrocytes comprise two populations differing in glutamate transporter and AMPA receptor expression. *J. Neurosci.* **21**, 7901-7908.